Local description of foam flow, deformation and pressure drop in narrow constricted channels

Badve, Mandar; Barigou, Mostafa

DOI:
10.1016/j.ijmultiphaseflow.2020.103279

Local description of foam flow, deformation and pressure drop in narrow constricted channels

Mandar Badve, Mostafa Barigou*

School of Chemical Engineering, University of Birmingham, Edgbaston, Birmingham B15 2 TT, United Kingdom

Abstract

We study in extensive detail the flow of dry and wet gas-liquid foams through a narrow two-dimensional channel comprising a complex constriction. The effects of constriction profile and size of aperture, foam flowrate, liquid holdup and liquid viscosity are experimentally investigated and a sophisticated image analysis procedure is developed to extract local fields of foam flow and deformation. Foam dynamics are scrutinised and interpreted in terms of local velocity distribution, elastic strain (texture tensor), plastic deformation (T1 events) and pressure drop. Important foam transformations occur in the vicinity of the constriction. For the first time, the relationship between pressure drop, flowrate and size of constriction aperture is investigated.

Keywords: Foam flow, constriction, elastic deformation, T1 events, pressure drop, friction factor.

*Corresponding author - email address: m.barigou@bham.ac.uk

1. Introduction

Applications of gas-liquid foams and solid foams are numerous; they include polymers, food, consumer goods, beauty care, pharmaceuticals, ceramics, foamed concrete, firefighting, oil recovery and mineral particle transport. Recently, new applications have emerged in the medical field, e.g. foam-sclerotherapy for varicose veins, and expanding polymer foam for treating brain aneurysms. Currently the global annual market is approximately $61.9 billion for polyurethane foam (RAM, 2018), $8 billion for shaving foam (Choudhry, 2017), and $74 billion for ice cream (RAM, 2013). Despite these large markets, industrial practice and processes are neither efficient nor optimal because of a severe lack of fundamental understanding of foam science.

Gas-liquid foams are complex structured fluids: they are compressible, non-linear viscoelastic materials; their viscosity is much larger than for the liquid constituent, and they usually exhibit a high zero-shear viscosity which can be mistaken for a yield stress (Barnes, 1999; Jabarkhyl et al., 2020). Understanding of foam properties is therefore limited – design and control for applications is more art than science – and many issues remain unaddressed/unresolved, e.g. flow dynamics, structural behaviour, stability/metastability, and dependence of rheological properties on structure and physicochemical constitution; the recent *Deepwater Horizon* (*BP*) oil spill (Gulf of Mexico, 2010), caused by the failure of a pumped foamed cement, is an example of such a rheological challenge.

Liquid foams are also precursors for solid foams, e.g. food, polymer, concrete, ceramic and metallic; the science of gas-liquid foams is, thus, highly relevant to solid foam structure, both closed- and open-cell. There are two well-described limiting gas-liquid foam structures: (*i*) 'wet' foams have high liquid content and mostly spherical bubbles, e.g. ice cream, with up to ~ 50% continuous phase; (*ii*) 'dry' foams have polyhedral cells and low liquid content, e.g. polyurethane, ~ 5% continuous phase. Bubble size generally ranges from about 10 μm to several mm.

A number of limited empirical studies have been done on bulk foam flow in pipes (Barigou et al., 2003; Deshpande and Barigou, 2000), and recent preliminary experiments and simulations on flow through constrictions have concentrated on idealised two-dimensional foams (Jones et al., 2011). These complex geometries can have significant effects on foam structure and the flow regime, and may destabilise foam structure, giving morphological transformations (Deshpande and Barigou, 2001a, 2001b). For example, the industrial process of foam extrusion, or discharge from a pressure vessel, can change foam texture by (*i*) changes in gas volume fraction and/or bubble growth; (*ii*) flow induced bubble coalescence/aggregation; and (*iii*) changes in liquid phase bulk and surface rheology. These phenomena are not fully understood but are crucial in food processing, e.g. for ice cream flowing through a nozzle. They are also important for flow in or filling of narrow vessels or channels

with complex cross sections. Thus a foam with inadequate rheological properties may not readily flow through narrow passages and constrictions, giving poor 'fill'. Examples include flow of aerated confectionary in narrow channels and complex moulds, filling of cavities with insulation foam, flow of foamed cement slurries in narrow oil-well annuli, filling of hollow aerofoil sections with polyurethane foam to make aerodynamic tethers for communication and geoengineering applications, and production of pre-insulated pipes for district heating.

Because 3D bulk foams are opaque, analysing the properties of a foam passing through complex passages is difficult. Therefore, typically for detailed analysis, experimental and numerical studies have used the flow of single layer of a foam, i.e. a monolayer of bubbles, confined between transparent walls. Such a setup has also been used to study the flow of other complex fluids including emulsions, gels or polymer solutions around obstacles or through constrictions (Langlois, 2014). Foam flow around an obstacle has been studied experimentally by Dollet and co-workers (Dollet et al., 2005; Dollet and Graner, 2007), allowing validation of a so-called 2D viscoelastoplastic model of foam rheology (Cheddadi et al., 2011). Detailed works on foam flow in complex passages are scarce. A few limited experimental/simulation studies have looked at 2D flow of foam through a sudden contraction followed by a sudden expansion where foam experiences both shear and extensional stresses (Dollet, 2010; Jones et al., 2011; Langlois, 2014).

Dollet (2010) in their experimental work (0.2 to 0.4 % liquid holdup) considered a sudden contraction (length = 2, 5, 15 cm; aperture = 1, 2.1, 3.2, 4.4 cm) and concluded that there is an essential coupling between local elasticity, plasticity and flow. Local elastic deformation (elastic strain) is computed using a texture (or elasticity) tensor *M*, following the definition of Aubouy et al. (2003), whereas local plastic deformation is represented in terms of so-called T1 events (neighbour bubble switching events). Jones et al., (2011) compared experimental results of dry foams (~ 0.5 % liquid holdup) through a sudden contraction (length = 3 cm; aperture = 3 cm) followed by a sudden expansion with predictions obtained from quasi-static simulations conducted using the finite-element Surface Evolver code (Brakke, 1992). Langlois (2014), on the other hand, used Durian's mechanistic Bubble model whereby Newton's equation of motion is solved for each individual bubble, using classical numerical techniques originally developed for Molecular Dynamics, (Durian, 1997) to simulate the flow of wet foam (10 % liquid holdup) through a constriction. Contrary to Surface Evolver, Durian's model treats bubbles as discs not as separate films, accounts for foam dynamic properties, is comparatively simpler to implement and requires less computational time. In conclusion, whereas Langlois' model is suitable for simulating wet/dynamic foams, Jones et al's is applicable to dry/quasi-static foams.

This paper reports on an extensive experimental investigation of foam flow behaviour and rheological response in a narrow 2D channel containing a constriction of variable geometry and dimensions including sudden and gradual contraction-expansion types. Foam behaviour is examined as a function of foam flowrate, constriction profile, size of constriction aperture, foam liquid holdup and viscosity of surfactant solution. The local effects on the flow field including foam morphology, topology and velocity distribution are analysed. We examine individual bubble motion and deformation using a texture tensor and record T1 neighbour-switching events, allowing us to obtain the local strain field and hence determine the transition from elastic to plastic response. We also study the local foam pressure drop across the constriction for the various flow conditions considered.

2. Materials and methods

2.1 Experimental setup and procedures

Foam flow experiments were conducted in a custom-made Hele-Shaw cell consisting of two 30 mm thick horizontal acrylic plates of 110 cm length and 30 cm width, as depicted in Figure 1a, separated by a uniform adjustable narrow gap so that one or several bubble layers of foam could be accommodated. Prehumidified Nitrogen gas was injected through a 1 mm diameter glass-capillary sparger whilst surfactant solution was injected using an Eldex 3HM piston pump (Cole-Parmer UK). Thus, disordered but nearly monodisperse dry or wet foam with liquid content in the range 1 – 20% was generated at the bottom of a vertical acrylic column and allowed to flow into the narrow 2D channel via an inlet pipe, and out of the channel via an outlet pipe downstream where it was collected and the foamate recycled. In all experiments, the area mean bubble diameter (d_{21}) was around 4 mm ± 1 mm and remained constant throughout the flow channel, i.e. no bubble coarsening or breakage occurred during the flow.

The uniform gap between the two acrylic plates in the Hele-Shaw cell was fixed at 3 mm to accommodate a single bubble layer of foam. To create a flow constriction, two identical constriction plates of thickness 3 mm were inserted and clamped down between the acrylic plates, as depicted in Figure 1b. The spacer plates and constriction plates were all made of black acrylic to minimise the effects of light reflection at edges. The Hele-Shaw cell was divided into two identical parallel flow channels using another 3 mm thick acrylic plate, thus, foam flowing into the gap divides into two identical mirror-image flows, as shown in Figure 1b. Thus, one channel was dedicated to measuring pressure drop at several positions 5 cm apart along the flow (including at the inlet, centre and exit sections of the flow constriction), using a sensitive strain gauge type micro-manometer capable of detecting gauge pressures down to 0.1 mm of water. The pressure tappings were each supplied with a side nitrogen gas bleed through a 0.5 mm capillary to prevent foam from flowing inside the tappings, without affecting the pressure readings, as successfully used in our previous work on foam flow in pipes (Deshpande and Barigou, 2001b, 2001a). The second flow channel, on the other hand, was used solely for visualisation of the foam flow, avoiding the obstruction caused by the pressure tappings.

Videos and images of foam flow were recorded using a Basler ace acA1300-200um camera at a rate of 100 to 200 frames per second.

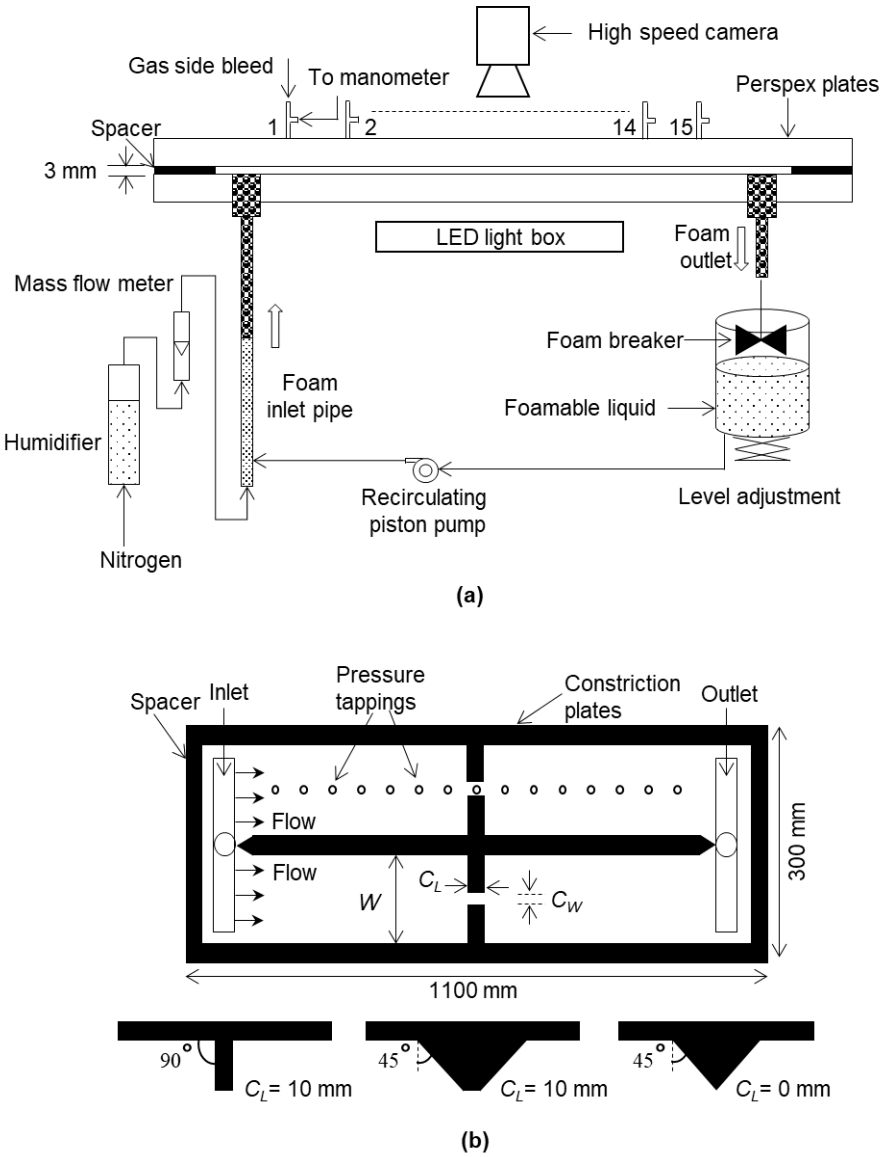

Figure 1. Schematic of Hele-Shaw cell foam flow rig: (a) side view; (b) top view and geometric details of the different flow constrictions used.

Three different flow constriction geometries were used: a sudden 90° contraction-expansion and two gradual 45° converging-diverging constrictions having different lengths (C_L = 0 and 10 mm) of the central constricted region (Figure 1b). The width of the flow channel is denoted by W and the width of the constriction (aperture) is denoted by C_W.

Foam was stabilised using technical grade Sodium Dodecyl Benzene Sulphonate (NaDBS, Sigma Aldrich UK), an anionic surfactant, at a concentration of 2.0 gL^{-1} (equivalent to 5 times its critical micelle concentration) to ensure a consistent surface tension throughout the flow system, dissolved in Type 2 water (equivalent to double distilled water). The surface tension of the NaDBS solution was 32.9 ± 0.1 mNm^{-1} and its viscosity was 1.04 ± 0.03 mPas. The liquid viscosity was varied by dissolving known amounts of glycerol in water.

Details of the foam flow experiments conducted are summarised in Table 1. Foam dynamics were studied in terms of local velocity distribution, elastic strain (texture tensor), plastic deformation (T1 events) and pressure drop. Sample videos of foam flow experiments are provided for illustration in the Supplementary Information section.

Experiment	**Angle of converging-diverging section**	**Size of constriction aperture (C_W), mm**	**Length of constriction (C_L), mm**	**Foam flowrate (Q_F), mL.min^{-1}**	**Foam liquid holdup (ε_L), %**	**Viscosity of surfactant solution (μ_L), mPa.s**
Reference case	90°	10	10	101.01	1	1.04
Effect of foam flowrate	90°	10	10	60.61-202.02	1	1.04
Effect of angle of converging-diverging section	45°, 90°	10	10	101.01	1	1.04
Effect of size of constriction aperture	45°	4, 7, 10, 15	0	101.01	1	1.04
Effect of foam liquid holdup	45°	10	0	101.01	3, 9, 15, 20	1.04
Effect of viscosity of surfactant solution	45°	10	0	101.01	1	1.04, 30.1, 44.7

Table 1: Experimental details

2.2 Foam flow image analysis

The well-known imageJ software was used for image processing (Eliceiri et al., 2012). A typical raw image of a foam flowing in the narrow channel is shown in Figure 2a. Figures 2b-c show the steps required to convert the raw image into a network of one-pixel-thick edges (skeletonised image). We first invert the grey levels of the raw image, then threshold them to separate the black

network of bubble edges from the white background to make a binary image (black and white; Figure 2b). Different zones on the image are treated with different thresholds to compensate for spatial variations in light intensity. In the final step, we "skeletonize" the foam to a network of edges one-pixel-thick (Figure 2c). The same skeletonisation process was used for both dry and wet foams. However, for wet foams, thresholding and binarisation of each image was done using a different imageJ algorithm depending on the liquid holdup, to account for the thick edges of the foam. This process preserves the topology of the foam, ensuring a faithful representation of the real foam which can be used to analyse the dynamics of foam flow in terms of local velocity distribution, texture tensor and T1 events. Another possible approach was to use Voronoi Tesselation to skeletonise the images (Graner et al., 2008) but this yielded the same results. More details on the imageJ software can be found in the ImageJ User guide (Ferreira and Rasband, 2012).

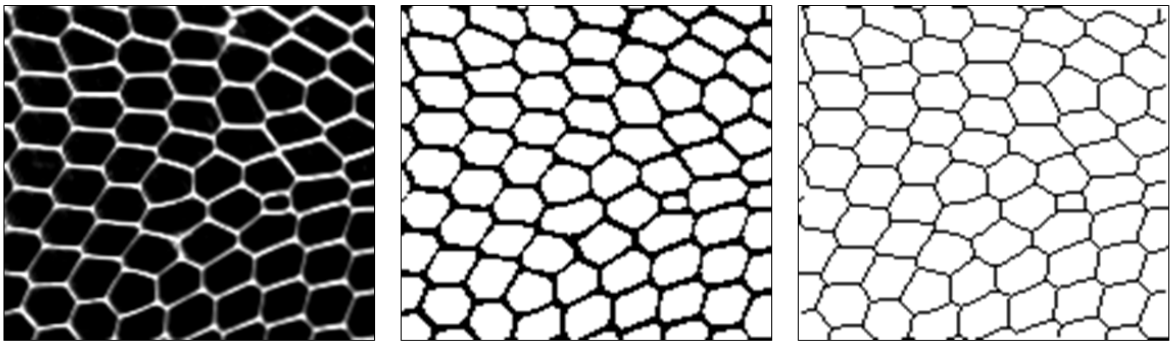

(a) (b) (c)

Figure 2. Foam image analysis: (a) raw image; (b) binary image; (c) skeletonized image.

2.3 Calculation of relevant foam flow fields

2.3.1 Local velocity distribution

To measure the local velocity distribution of a foam flowing through a narrow channel with a constriction, we utilised a standard cross-correlation algorithm that is used in the imaging technique of Particle Image Velocimetry (PIV). A white LED light box of dimensions 30 cm × 20 cm was placed below the flow channel to illuminate the foam. In PIV, microscopic tracer particles are used to track the motion of a fluid. In foam flow, tracer particles are not needed since the bubble interfaces in the moving foam themselves scatter light. PIVlab (Thielicke and Stamhuis, 2014), a time-resolved digital Particle Image Velocimetry toolbox available in MATLAB, was used to analyse the skeletonized images. Initial tests revealed that the optimum number of images to be analysed in each experiment was 4000 to avoid statistical bias, and beyond which the mean local velocity distribution was unaffected by the number of images analysed. Multi-pass interrogation windows (four in this case) of size ranging from 50×50 pixels to 20×20 pixels were used in the cross-correlation algorithm. The smallest interrogation window size was slightly larger than the average individual bubble area.

2.3.2 Texture tensor

To analyse the local foam cell deformation, we compute following the definition of Graner et al. (2008) a texture (or elasticity) tensor M which provides an operational definition of deformation which can be experimentally measured and given in terms of averages of microscopic quantities. This was an improvement on previous work by Aubouy et al. (2003) who had used bubble edges rather than the link between neighbouring bubbles, as detecting bubble centres is more accurate. The magnitude of the texture tensor measures the elastic strain of the pattern formed by the bubbles. Considering the link between two neighbouring bubbles to be the vector $v = \binom{x}{y}$, the texture tensor is then defined as:

$$M = \langle v \times v \rangle = \begin{pmatrix} \langle x^2 \rangle & \langle xy \rangle \\ \langle xy \rangle & \langle y^2 \rangle \end{pmatrix}. \quad (1)$$

To find the links between neighbouring bubbles on imageJ, the positions of the bubble centres are extracted using an in-house image processing algorithm, followed by a Delaunay triangulation of bubble centres (Ferreira and Rasband, 2012). It should be noted that Jones and Cox (2012) used direct links between bubbles in foam simulations and the Delaunay triangulation in analysing experimental data; the results were indistinguishable. Furthermore, to identify the direct links, one needs to check that the bubbles are touching when defining a link (not always the case in a wet foam). The Delaunay triangulation which requires less computational effort, will also put links in whenever bubbles are close, which are important advantages. Once all such links are identified, using a separate in-house C++ algorithm, each image is divided into a number of interrogation boxes and averaging of triangulated network movement (displacement in x and y direction) is done over all links found in a given box during a given time to compute the tensor in each box. Each local tensor is depicted by an ellipse (Figure 3) whose major and minor axes represent, respectively, the foam cell elongation vector and compression vector.

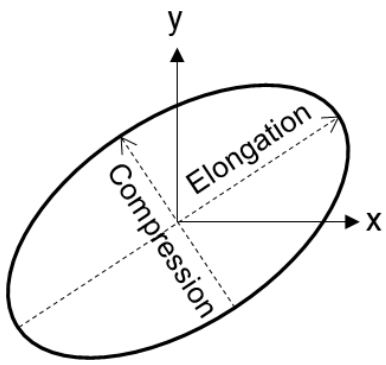

Figure 3. Ellipse representing local texture tensor: major axis represents foam cell elongation vector and minor axis represents its compression vector.

To quantify the elastic strain in the foam, we consider the relevant components of the texture tensor M, i.e. the normal components M_{xx} and M_{yy}, to obtain the normal strain difference M_{xx} - M_{yy}. Since the elastic strain scales as a characteristic bubble size, we rescale the normal strain difference by the trace $M_{xx} + M_{yy}$ to compare different bubble areas, as the latter depends on the gas flowrate (Jones et al., 2011). The normal component of the elastic strain or normalised texture tensor component is thus defined as:

$$M_n = \frac{M_{xx} - M_{yy}}{M_{xx} + M_{yy}}. \tag{2}$$

The value of M_n signifies the total extensional strain in the foam and is a more useful parameter for comparing bubble deformation.

2.3.3 T1 events

A T1 topological transformation also called T1 event is a neighbour swapping event, i.e. a local plastic rearrangement between bubbles, in which one of the soap films between neighbouring bubbles vanishes and a new film forms. Figure 4 shows a schematic representation of a T1 event: initially, bubbles 2 and 4 are neighbours, but due to external deformation the film separating them (marked in red colour) shrinks in length, resulting in an unstable 4-fold vertex before forming a new film (marked in blue colour). In order to determine the location of T1s we seek four-fold vertices in the experimental images. We then calculate the frequency of T1s and their distribution across the length and width of the flow channel including the constriction region. The distribution and frequency of T1 events provide a local measure of plasticity for foam flowing through 2D narrow channels, thus, highlighting regions where foam is likely to undergo plastic deformation and elucidating how flow dynamics and flow geometry can affect its plasticity.

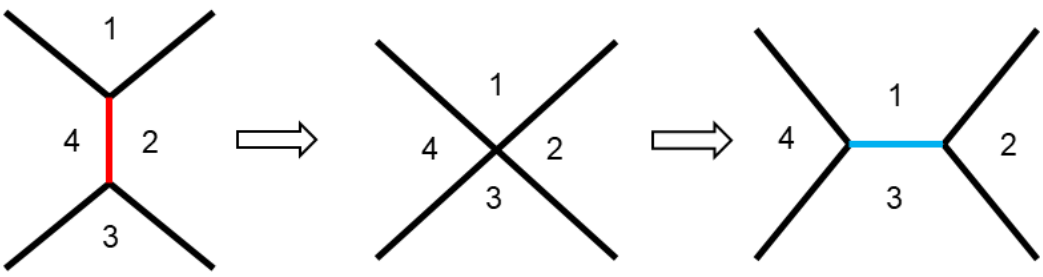

Figure 4. Schematic representation of a T1 event between four neighbouring bubbles: red film disappears and blue film emerges resulting in neighbour bubble switching.

3. Results and discussion

We first focus on discussing in detail our reference case experiment: the flow of a nearly monodisperse foam with flowrate 101.01 mLmin^{-1} in the 90° constriction with C_L = 10 mm and ε_L = 1.0%. We then examine the influence of each control parameter listed in Table 1. Results are mainly reported inside an observation window of 10 cm either side of the constriction where the important foam transformations occur.

3.1 Reference case experiment

3.1.1 Velocity field

The full velocity field corresponding to the reference case experiment described above, is depicted in Figure 5. Even at this low flowrate (foam velocity well upstream of the constriction ~ 3 mm/s), no dead zones are observed anywhere in the flow channel. This is in contrast with the flow of viscoplastic fluids (with an apparent yield stress) where dead zones are a common feature (Jay et al., 2002). This confirms that such foams do not possess a yield stress, which is consistent with rheological measurements of various surfactant and protein stabilised foams reported in the literature (Barnes, 2000; Lim, 2005; Jabarkhyl et al., 2020), and contrary to a number of previous presumptions (see for example, Dollet, 2010; Cheddadi et al., 2011; Langlois, 2014). Similar velocity vector maps were reported in experiments with 2D dry foams (ε_L ~ 0.4%) by Dollet (2010) and with wet foams (ε_L ~ 10%) by Langlois (2014). As the foam approaches the constriction, the local velocity increases because of the reduction in flow area. It reaches its maximum value in the middle of the constriction (narrowest section), decreasing thereafter downstream as the area of flow expands (by virtue of mass continuity), as demonstrated by the velocity profile along the central axis of the flow channel plotted in Figure 6a. The divergence of the velocity field is zero well upstream and downstream of the constriction implying that the foam does not manifest its compressibility in these regions. Immediately before reaching the constriction (x ~ – 1.5 cm), however, the divergence turns negative reaching a minimum (~ – 0.5 s^{-1}) at the inlet, and starts to increase again to become positive just before the exit, reaching a maximum (~ + 0.8 s^{-1}) just after the exit (x ~ 0.75 cm), implying compressible flow in the entire vicinity of the constriction with considerable foam density variations as confirmed from mass continuity. There is a small undershoot in the velocity downstream of the constriction. The observed foam compressibility in the vicinity of the constriction and bubble elasticity (elastic deformation of bubbles in transverse direction) might be the prime factors responsible for such undershoot of velocity along central axis. This undershoot has also been observed in the flow of 2D dry foams experimentally by Dollet (2010) and in simulations by Jones and Cox (2012). This type of velocity profile was characteristic of all the experimental cases studied here.

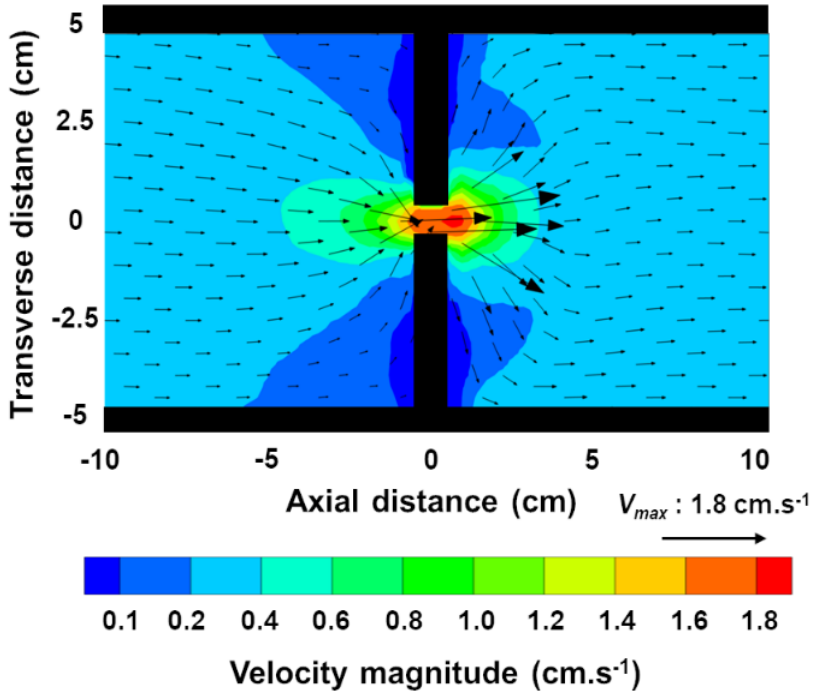

Figure 5. Velocity field in foam flowing through a sudden 90° constriction.

Transverse velocity profiles are also plotted across the channel (y = –4.5 cm to 4.5 cm), upstream of the constriction in Figure 6b and downstream of it in Figure 6c. There is almost plug flow at the entrance of the observation window (x = –8 cm) as there is little variation in velocity across the width of the channel. As the foam approaches the constriciton, the velocity profile is increasingly impacted by the presence of the constriction, becoming very sharp at x = –1 cm. The effects of the constriction on the velocity profile are approximately reversed, although there is significant asymmetry in the velocity distribution, as the foam leaves the constriction and moves downstream (Figure 6c); there is first an acceleration at the exit (x = 1 cm) leading to a velocity much higher than at the inlet (x = –1 cm), followed by a rapid deceleration leading to the velocity undershoot highlighted above and then recovery to mirror the plug flow upstream of the constriction.

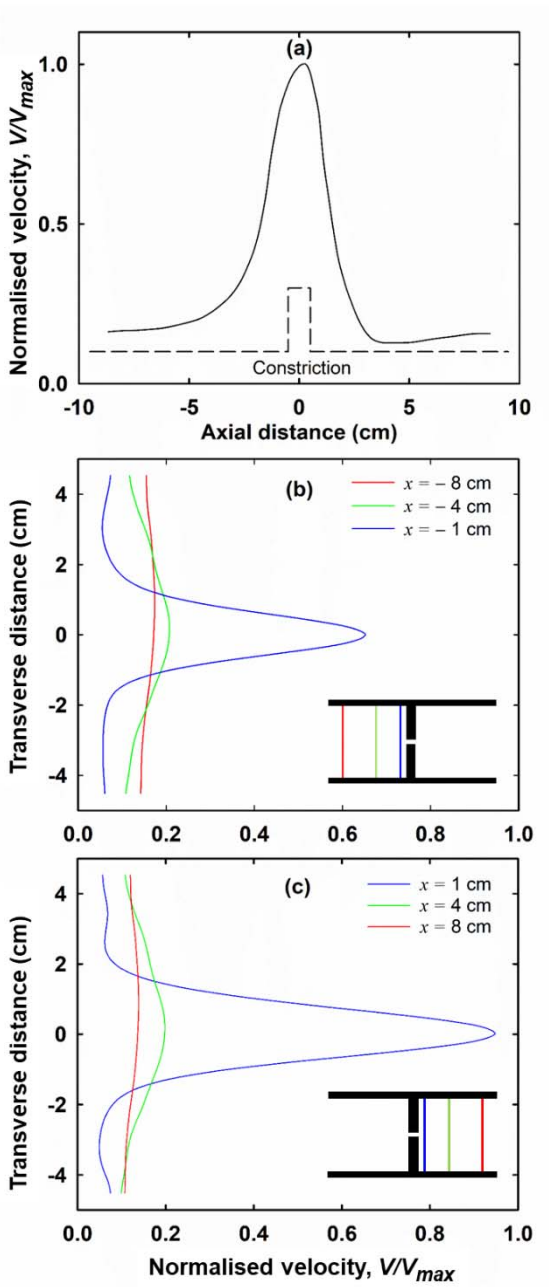

Figure 6. Normalised velocity profiles in sudden 90° constriction: (a) velocity along the central axis of the flow channel; (b) transverse velocity across the width of the flow channel upstream for the constriction; (c) transverse velocity across the width of the flow channel downstream for the constriction.

3.1.2 Elasticity/Texture tensor

To quantify bubble deformation in the reference case experiment, we calculate the texture tensor M defined in Equation (1), and use our ellipse representation (Figure 3) to depict the entire elastic strain field in Figure 7a and plot the normal component M_n in Figure 7b. Bubbles begin to elongate in the spanwise direction at significant distances upstream of the constriction. Comparing the individual components of M_n (data not shown) shows that bubble elongation increases whereas

compression decreases, but both increase as the foam approaches the constriction. Such a deformation increases sharply as the foam moves forward reaching a maximum inside the constriction where $M_n \approx 0.52$. Here, bubble elongation and bubble compression (not to be confused with flow compressibility) measured from the individual components of the texture tensor, both increase sharply but elongation dominates by far. Qualitatively similar findings were independently reported by Jones et al. (2011) and by Dollet (2010) for the flow of dry foams ($\varepsilon_L \sim 0.2$-0.4%) in abrupt constrictions of different length and aperture sizes, including interestingly a similar maximum value of $|M_n|$ (~ 0.5).

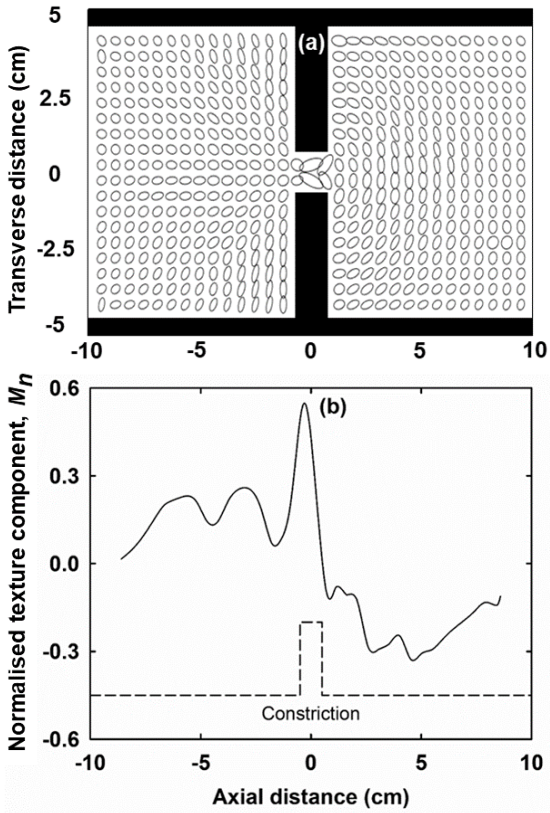

Figure 7. Variations of local texture tensor throughout the flow channel in sudden 90° constriction: (a) ellipse representation of M; (b) axial variations of M_n.

At the exit section of the constriction, however, both elongation and compression suddenly decrease. There is a brief bubble relaxation followed by an abrupt inversion of the elastic strain in the (negative) transverse direction which continues to increase in magnitude over a distance of a few centimetres. Since bubbles extend spanwise before the constriction, the value of M_n is positive ($M_{xx} > M_{yy}$). Similarly, because the bubbles extend streamwise after the constriction, the value of M_n is negative ($M_{yy} > M_{xx}$). This change in sign occurs exactly at the exit of the constriction, indicating a change in the direction of deformation; elongation increases again and compression decreases, both eventually reaching steady state further downstream. The fluctuations in the average value of M_n, upstream and downstream of the constriction result from the non-uniform flow near the constriction

and the random rearrangements between bubbles in the form of T1 events. Bubble deformation downstream appears to be slightly lower than upstream. Finally, a gradual elastic relaxation begins tending towards equilibrium, i.e. bubbles tend towards a circular shape beyond a distance of approximately 5 cm with M_n rising towards zero (Figure 7ab). This relaxation phase continues outside the observation window, reaching completion near the exit of the channel.

3.1.3 T1 events

Figure 8a shows the local distribution of T1 events over a time interval of 10 s in the reference case experiment, describing the local plastic deformation of the foam. T1 events are concentrated in the vicinity of the constriction where all the significant topological transformations tend to occur, and their number increases with time. Hardly any T1 events were observed far upstream and downstream of the constriction near the edges of the observation window. The distribution of T1 events seems to differ slightly from that reported by Dollet (2010). Such a difference could be due to a variety of factors including the fact that the size (C_W) of the aperture of their constriction was considerably larger than the one used here.

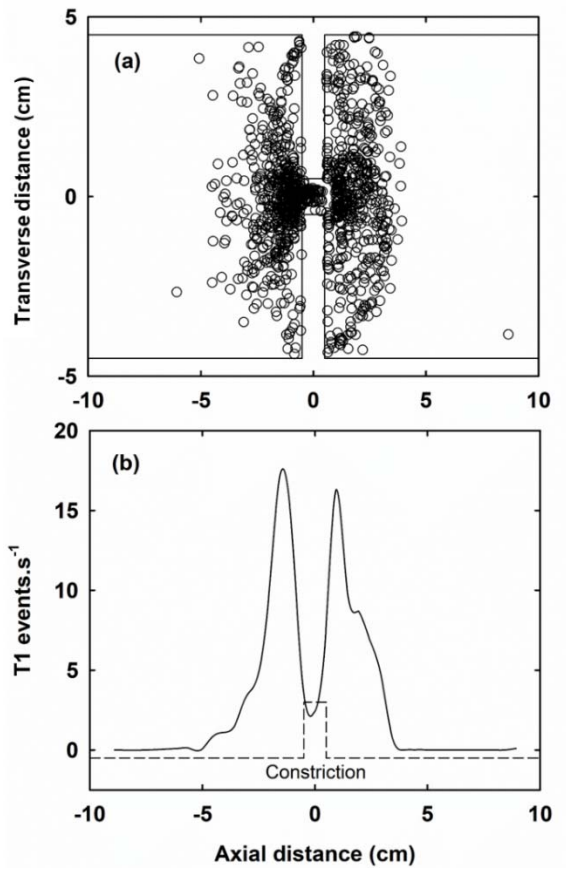

Figure 8. Distribution of T1 events in sudden 90° constriction during a 10 second time interval: (a) Local distribution of T1 events; (b) Axial variation of total T1events frequency.

T1 events detected inside narrow vertical bands (4-8 mm wide) across the channel were summed up and a local T1 frequency was obtained by dividing the total by the observation time (10 s), and results are plotted in Figure 8b. Two sharp peaks were observed, just before the constriction and just after, separated by a narrow zone (~ 5 mm) inside the constriction where only a small number of T1 events are detected. As the foam approaches the constriction, bubbles rearrange to squeeze through, resulting in a high occurrence of T1 events and high elastic deformation (see section 3.1.2) confirming the strong link between local plasticity (T1 events) and elastic strain (texture tensor) (Marmottant et al., 2008). Similarly, downstream in the expanding section of the constriction, bubble elongation and rearrangement lead to a high T1 frequency mirroring approximately the behaviour upstream. The T1 frequency profile is consistent with results reported by Dollet (2010) and by Langlois (2014).

3.2 Effects of control parameters

In this section, we study the influence of the various control parameters (Table 1) and we, therefore, scrutinise the variations of the relevant components of the fields along the length of the channel including the normalised local velocity, normalised component M_n and the frequency of T1 events.

3.2.1 Effects of foam flowrate

The influence of foam flowrate (60.61-202.02 mL.min^{-1}) was investigated using a 90° constriction with C_L = 10 mm and ε_L = 1.0%. Lower flowrates than these would lead to very small constriction effects on the foam, whilst higher flowrates would lead to the generation of polydisperse foams which are not the focus of this work. Figure 9a shows V/V_{max} along the centreline of the flow channel and the curves almost collapse onto a single master curve, implying that the normalised velocity distribution is independent of flowrate. The velocity undershoot downstream of the constriction, previously observed in the reference case experiment (Figure 6a), reduces with flowrate.

The variations of M_n along the centreline of the flow channel are depicted in Figure 9b. As the foam flowrate increases, the maximum value of M_n near the constriction also increases gradually by ~ 35% over the whole range, indicating that the bubbles incur more deformation inside the constriction at higher flowrates. However, there is no obvious trend in the variations of M_n upstream and downstream of the constriction.

Figure 9c shows the frequency of T1 events along the channel for different foam flowrates. There are consistently two major peaks, one peak just before the constriction and one just after. These two peaks are separated by a narrow zone (~ 5 mm) inside the constriction with negligible T1 occurrences. The total number of T1 events within the observation window increases approximately linearly as a function of flowrate (Figure 9c); this seems to confirm the earlier prediction by Langlois

(2014). An increase in flowrate results in an increase in local strain, which ultimately triggers more T1 events.

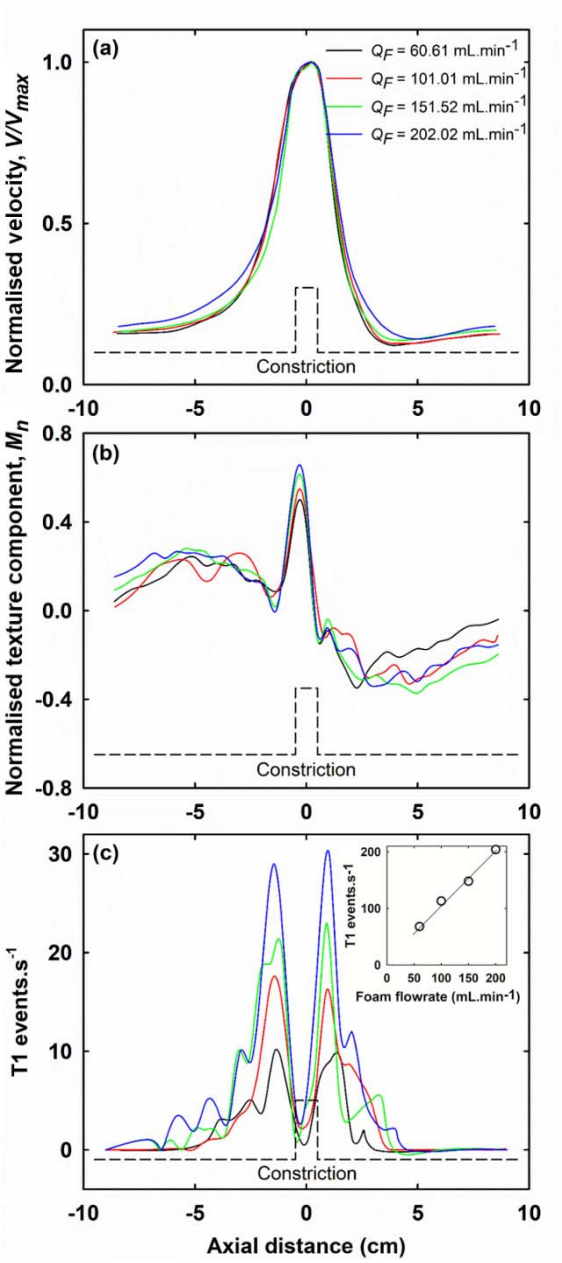

Figure 9. Effects of foam flowrate on: (a) normalised local velocity; (b) normalised texture component; (c) frequency of T1 events.

3.2.2 Effects of constriction profile

To study the influence of constriction profile, experiments were conducted using two 45° and 90° constrictions both having C_L = 10 mm (Figure. 1b) at a fixed foam flowrate of 101.01 mL.min^{-1} giving ε_L = 1.0%. Features of the flow through the two constrictions are compared in Figure 10. Surprisingly, the velocity curves do not exhibit any major differences. The undershoot observed at the exit in case of the sudden constriction is much less pronounced in case of the gradual constriction.

Again, the constriction profile does not have a major impact on the normalised texture component except for the elastic recovery downstream ($M_n \rightarrow 0$) which is much faster for the sudden constriction. There are, however, significant differences in the frequency of T1 events occurring in the vicinity of the constrictions. The peaks just upstream and just downstream of the constriction are much higher for the sudden constriction, and the total number of events is almost double (Figure 10c-e). In the case of the 90° constriction, because of the sudden variation in the area of flow, bubbles experience a higher local strain which results in approximately a doubling of topological changes; however, such rearrangements drop to zero quickly downstream.

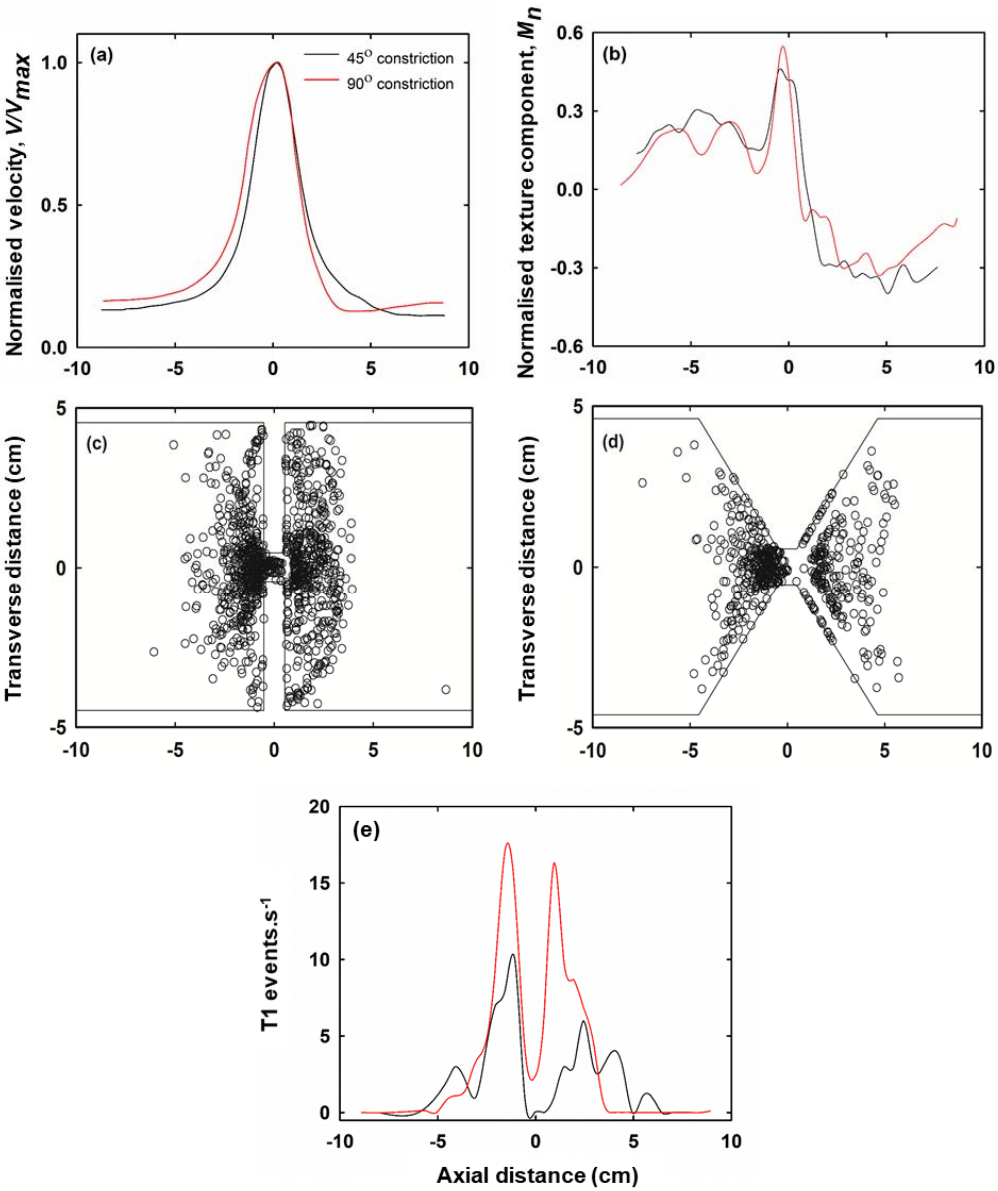

Figure 10. Effects of constriction profile on: (a) normalised local velocity; (b) normalised texture component; (c) local distribution of T1 events in 90° constriction; (d) local distribution of T1 events in 45° constriction; (e) frequency of T1 events.

3.2.3 Effects of size of constriction aperture (C_W)

To study the influence of the size of the constriction aperture (C_W), we image foam with ε_L = 1.0% flowing at 101.01 mL.min^{-1} through a 45° constriction with C_L = 0 mm (Figure 1b), but varying C_W from 4 to 15 mm, whilst the bubble size was constant with d_{21} = 4 ± 1 mm. The axial velocity profiles shown in Figure 11 collapse approximately on a single curve irrespective of the constriction aperture size.

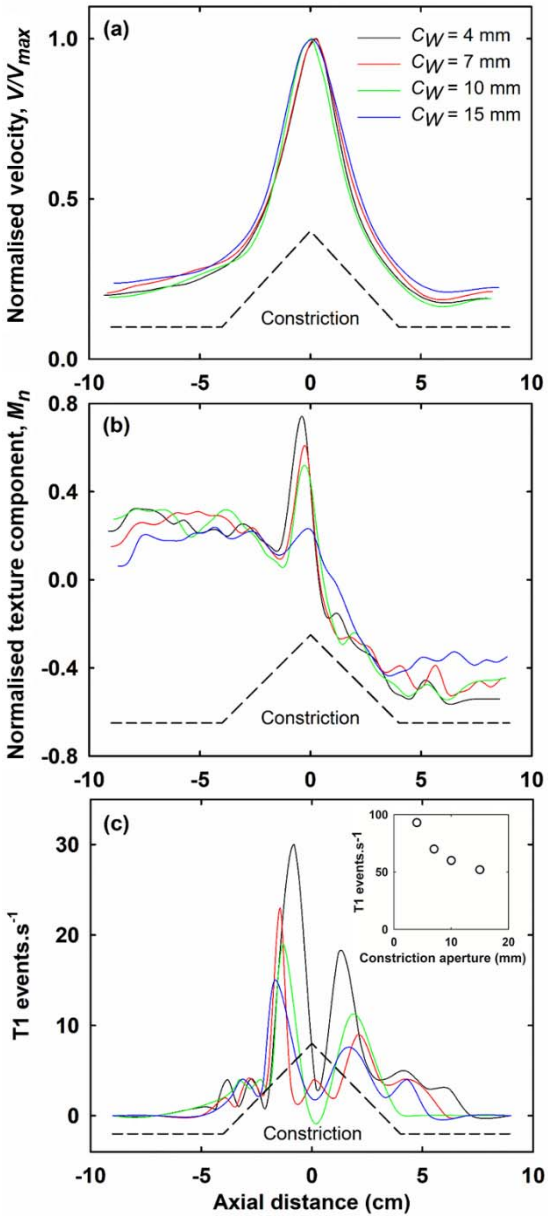

Figure 11. Effects of size of constriction aperture (C_W) on: (a) normalised local velocity; (b) normalised texture component; (c) frequency of T1 events.

The main differences between the M_n profiles occur at the centre of the constriction, showing increasing elastic deformation for narrower apertures. For all constrictions, M_n falls off rapidly to

zero as the foam leaves the constriction, changes sign and continues to increase in magnitude before reaching a plateau with bubbles emerging from narrower constrictions exhibiting more deformation; eventually M_n is expected to rise to zero near the exit of the channel. The greater the C_W value the smaller the total number of T1 events (Figure 11c). As the size of the constriction aperture increases, the foam undergoes less deformation and hence less T1 events are observed.

3.2.4 Effects of foam liquid holdup

The effects of the foam liquid holdup (1.0% – 20%) was investigated using a foam flowing at a fixed flowrate of 101.01 mL.min^{-1} through the 45° constriction with C_L = 0 mm (Figure 1b). Within the conditions investigated, varying ε_L did not produce any significant effect on the axial velocity profile, as shown in Figure 12a. On the other hand, the transverse velocity profiles depicted in Figure 12b, show considerable differences. These velocity profiles become flatter (i.e. tends to plug flow) as ε_L increases. We express the overall uniformity of such profiles using the uniformity index I:

$$I = \frac{\sum w_i}{n} \tag{3}$$

where, $w_i = \frac{\sqrt{(V_i - \bar{V})^2}}{\bar{u}}$ is a measure of local uniformity; V_i is the local velocity at location i and $\bar{V}$ is the mean velocity at n locations across the flow channel at x = – 8 cm. For ideal plug flow, I = 0. As ε_L increases from 1.0% to 20%, I reduces from 0.042 to 0.008, approaching zero. Thus, in contrast to dry foams, wetter foams tend to approach the constriction in the plug flow regime. The same behaviour was observed downstream, as the foam moved away from the constriction. With an increase in liquid holdup, the Plateau borders sliding on the wall become thicker, hence, causing less sliding friction which is consistent with pressure drop measurements (section 3.3). In consequence, as shown in Fig. 12c, this reduces elastic deformation in the foam and, hence, velocity variations also reduce, tending towards plug flow. Plug flow was observed in wet foams flowing in pipes (Deshpande and Barigou, 2000).

The variations of M_n depicted in Figure 12c show that dry foams experience significantly more deformation than wet ones inside the constriction as well as upstream and downstream of it. With more liquid present in foam, the lubricating liquid layer on the wall is thicker, thus, reducing the wall sliding friction, i.e. the wall shear stress and, hence, the elastic strain. Using numerical simulations, and in agreement with experimental findings from the literature, Marmottant *et al*. (2008) concluded that elastic deformation in foams flowing past obstacles decreased with liquid holdup. Cheddadi et.al (2011) who studied flow of foams past obstacles experimentally, also reported more elastic deformation (twice the maximum M_n value) in the case of a dry foam (ε_L =1.2 %) compared to

a wetter foam (ε_L =7 %). The frequency of T1 events (Figure 12d), however, does not show a clear trend; as ε_L increases, it remains more or less the same.

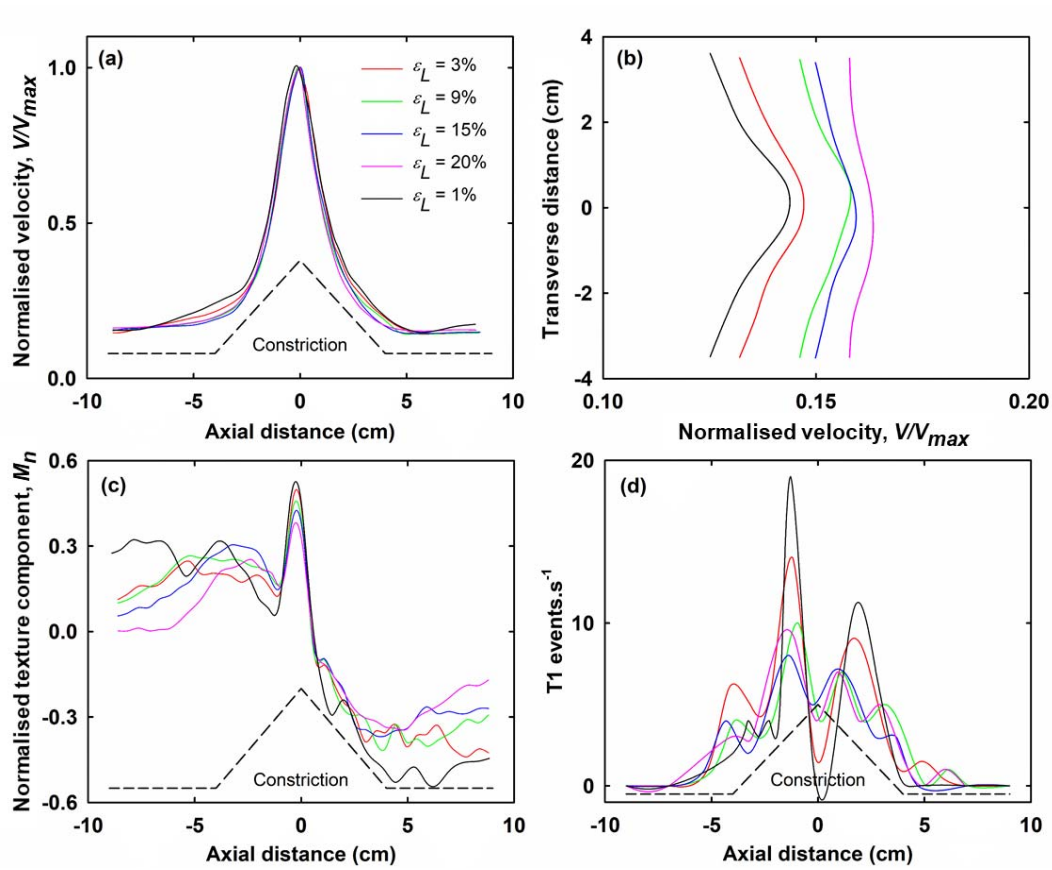

Figure 12. Effects of foam liquid holdup (ε_L) on: (a) velocity along the central axis of the flow channel; (b) velocity across the width of the flow channel at x = - 8cm; (c) normalised texture component; (d) frequency of T1 events.

3.2.5 Effects of viscosity of surfactant solution

The viscosity of the surfactant solution (μ_L) was varied within the range μ_L = 1.04 – 44.7 mPa.s, using the 45° constriction with C_L = 0 mm (Figure 1b) at a fixed flowrate of 101.01 mL.min^{-1} (ε_L = 1.0%). Within the conditions investigated, varying μ_L did not produce any significant effect on the axial velocity profile, as shown in Figure 13a. There are no discernible effects on M_n upstream of the constriction (Figure 13b). However, as the foam interacts with the constriction, foams formed from more viscous liquids experience significantly less elastic deformation, positive inside and negative on exit of the constriction; the rate of liquid drainage in the Plateau borders slows down making them and the liquid films slightly thicker, thus, probably enhancing inter-bubble mobility/slippage and reducing deformation (Deshpande and Barigou, 2000). Whilst lower viscosity

foams seem to incur more T1 transformations at the inlet of the constriction and less inside, such differences vanish as the foam leaves the constriction (Figure 13c).

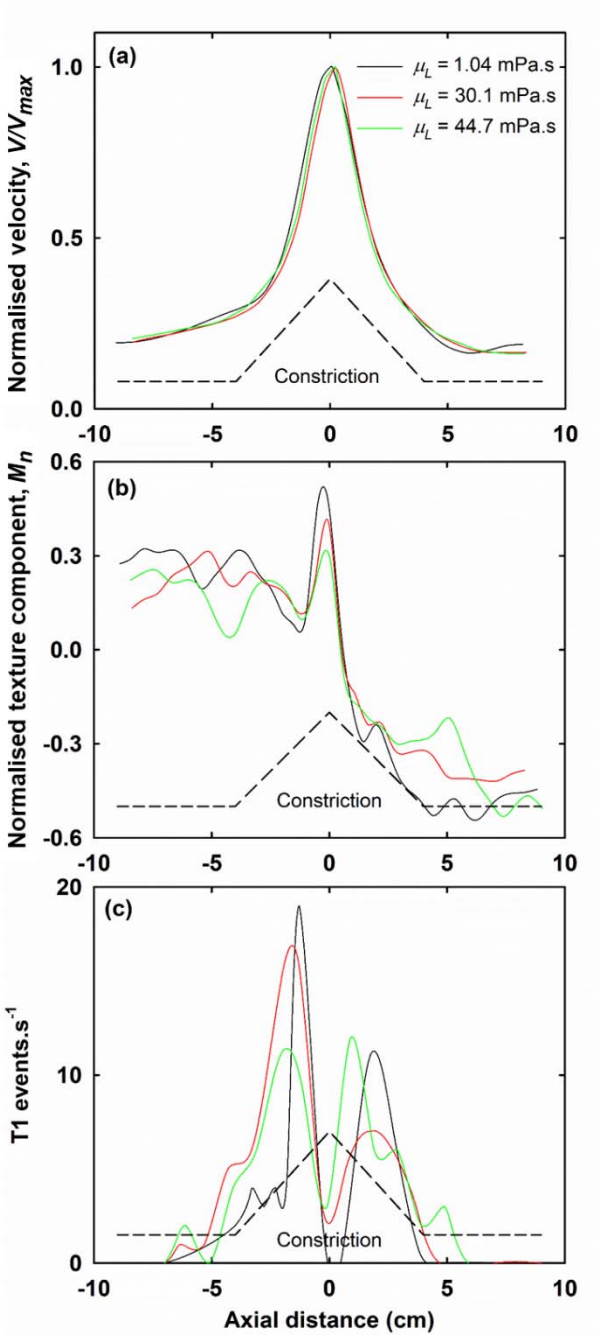

Figure 13. Effects of viscosity of surfactant solution on: (a) normalised local velocity; (b) normalised texture component; (c) frequency of T1 events.

3.3 Pressure drop in foam flow

Pressure drop was measured along the whole flow channel including the constrictions described in Figure 1b. Typical profiles are shown in Figure 14a for foam with ε_L = 1.0%, and a 45° constriction (C_L = 0 mm, C_W = 10 mm). The Piezometric pressure varies approximately linearly along

the length of the channel both upstream and downstream of the constriction. There is a slight drop in the slope of the line downstream compared to upstream. The constriction causes a significant local pressure drop. The flow being horizontal, the entire pressure drop is attributed to the sliding friction at the walls of the channel. These results are consistent with earlier observations concerning the flow of bulk foams in pipes (Deshpande and Barigou, 2001b, 2000; Wiggers et al., 2000). The effects of varying the size of the constriction opening are depicted in Figure 14b. As expected, narrower constrictions generate much larger local pressure drops, but the trend is approximately linear as a function of foam flowrate for all constriction sizes. As discussed above (section 3.2.3), reducing the constriction opening leads to more intensive bubble rearrangements (i.e. more elastic strain and more T1 topological transformations) and, hence, more energy dissipation.

Foam pressure drop in the straight channel and across the constriction also varied as a function of constriction profile, foam liquid holdup and liquid viscosity. Pressure drop results for flow through a sudden 90° constriction showed similar trends as the 45° constriction, but were 1.2 – 1.5 times higher (data not shown), depending on flow conditions. Across the constriction, this increased pressure drop may be attributed to the occurrence of more T1 events in a 90° constriction, causing more velocity fluctuations, thus, leading to more friction between bubbles and between bubbles and channel walls. Wetter foams experience less pressure drop, but a higher liquid viscosity leads to a higher pressure drop throughout the channel including the constriction. Such a pressure drop stems from the shear in the lubricating thin liquid film on the channel walls (Deshpande and Barigou, 2000). The wall film thickness cannot be readily measured but an effective thickness, δ, can be calculated from:

$$\tau_w = \frac{\mu_L V_F}{\delta} \tag{4}$$

where τ_w is the wall shear stress and V_F is the mean foam velocity. Values of δ = 1 – 10 μm were reported for foam flow in vertical pipes (Deshpande and Barigou, 2000). Our estimates of δ were in the range 5–40 μm depending on flow conditions. The higher values of δ may be due to the horizontal direction of the flow. A higher liquid holdup increases δ, which for a given surfactant solution viscosity and foam flowrate results in less pressure drop.

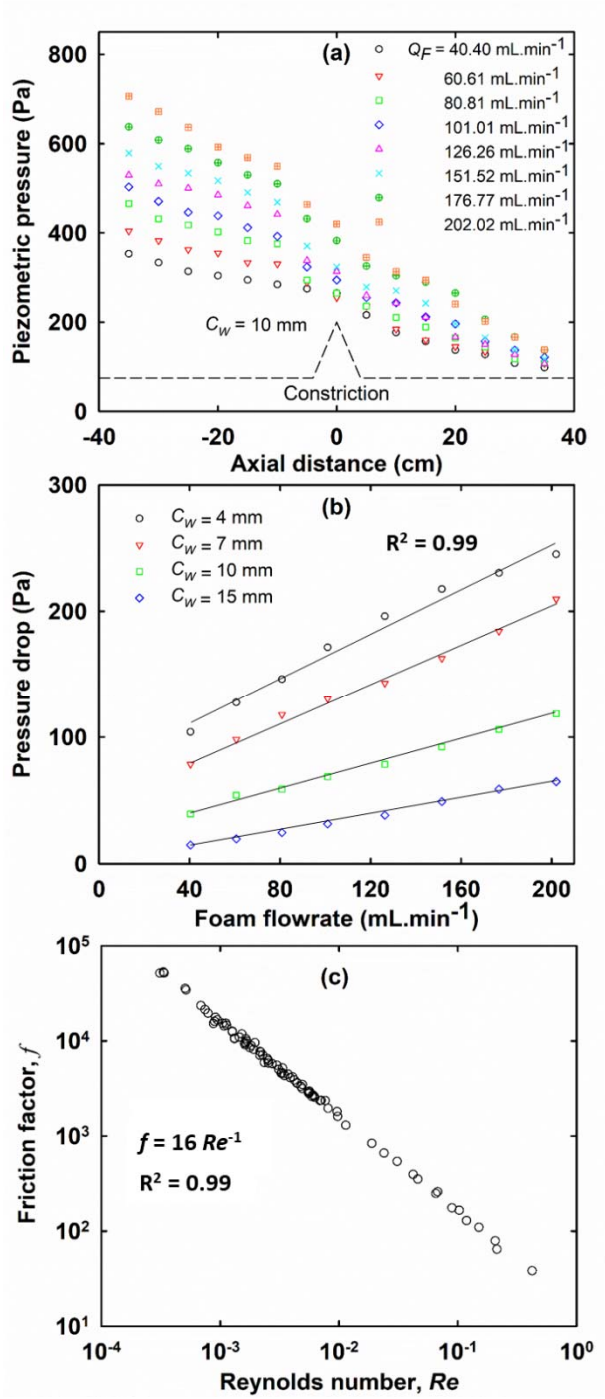

Figure 14. Pressure drop in foam flow with 45° constriction (C_L = 0 mm): (a) Piezometric pressure profile along the channel for different flowrates; (b) pressure drop across the constriction for different constriction apertures; (c) Fanning friction factor for foam flow in straight sections of the channel for different flowrates, constriction apertures, foam liquid holdup and viscosity of surfactant solution.

The straight sections of the flow channel contributed by far the largest part to the total pressure drop. The description of fluid flow by a friction factor is very useful for pressure drop calculations and the design and analysis of flow systems. As the motion of foam under the present conditions is mainly governed by the sliding action on the wall, the similarity between 2D and 3D flow can be reasonably assumed. Therefore, the approach of Deshpande and Barigou (2000), who

studied the pressure drop in foam flow through straight vertical pipes, is adopted here. The rheology of the foam flowing in the straight parts of the channel is described by considering the gas-liquid system as non-Newtonian pseudo-homogeneous fluid. Full details of the theoretical derivations can be found in Deshpande and Barigou (2000). It follows from this theory that for a foam obeying exact power-law rheology, the Fanning friction factor is given by $f = 16/Re$ where Re is the generalised Reynolds number given by:

$$Re = \frac{\rho_F V_F^{2-n} h^n}{2^{n-3} k \left(3+\frac{1}{n}\right)^n} \tag{5}$$

where h is the height of the flow channel, V_F is the mean foam velocity in the channel, ρ_F is the foam density determined from the mass flowrate of foam, and k and n are the power-law parameters. The friction factor data plotted in Figure 14c lie remarkably on a unique line and are well fitted by the expression:

$$f = \frac{16.0}{Re} \qquad (r^2 = 0.99) \tag{6}$$

where the power law model parameters obtained from the experimental data lie within the ranges: $0.1 \leq k \leq 0.21$ and $0.4 \leq n \leq 0.75$) Given that the foams studied here consist of a single bubble layer moving in a 2D channel, this shows that the relationship $f = 16/Re$ is universal for foam flow. This result has practical significance in that pressure drop in foam flow through a series of channels of different dimensions can be calculated using a constant friction factor.

4. Conclusions

Considering the entire foam flow field, no dead zones exist anywhere in the channel even at the slowest flowrates, confirming the non-existence of a yield stress. Important foam transformations occur in the vicinity of a flow constriction. The wetter the foam, the more it tends to approach the constriction in the plug flow regime. With an increase in foam flowrate and decrease in size of constriction aperture, foam pressure drop, local elastic strain and plasticity increase. More pressure drop and local plastic deformations are manifested across a 90° constriction compared to a 45° constriction, but downstream of the constriction, foam relaxation is faster. A higher liquid holdup and liquid viscosity reduce both local elastic and plastic deformations. There is a strong link between local plasticity (T1 events) and local elastic strain (texture tensor); a high elastic strain translates into a high plastic deformation. Such a transition occurs in the vicinity of the constriction. A higher foam liquid holdup increases the thickness of the lubricating liquid film on the wall, which for a given

liquid viscosity and foam flowrate results in less pressure drop. Pressure drop through straight narrow channels can be predicted using a constant friction factor. The relationship established here between pressure drop, flowrate and aperture size is a novel result which is of great importance to industrial applications, and could not be investigated in previous quasi-static foam studies.

Acknowledgments

This work was funded by EPSRC Grant EP/N002075/1. We are grateful to Prof. Simon Cox, Department of Mathematics, Aberystwyth University, UK, for useful discussions on texture tensor calculations.

References

Aubouy, M., Jiang, Y., Glazier, J.A., Graner, F., 2003. A texture tensor to quantify deformations. Granul. Matter 5, 67–70. https://doi.org/10.1007/s10035-003-0126-x

Barigou, M., Deshpande, N.S., Wiggers, F.N., 2003. Numerical Simulation of the Steady Movement of a Foam Film in a Tube. Chem. Eng. Res. Des. 81, 623–630. https://doi.org/https://doi.org/10.1205/026387603322150471

Barnes, H., 2000. A Handbook of Elementary Rheology. University of Wales, Institute of Non-Newtonian Fluid Mechanics.

Barnes, H.A., 1999. The yield stress—a review or 'παντα ρει'—everything flows? J. Nonnewton. Fluid Mech. 81, 133–178. https://doi.org/10.1016/S0377-0257(98)00094-9

Brakke, K.A., 1992. The Surface Evolver. Exp. Math. 1, 141–165. https://doi.org/10.1080/10586458.1992.10504253

Cheddadi, I., Saramito, P., Dollet, B., Raufaste, C., Graner, F., 2011. Understanding and predicting viscous, elastic, plastic flows. Eur. Phys. J. E 34, 1–15. https://doi.org/10.1140/epje/i2011-11001-4

Choudhry, K., 2017. Lindal's Actuator Targets the Shaving Gel and Foam Market [WWW Document]. URL https://www.beautypackaging.com/issues/2017-10-01/view_design-center/lindals-actuator-targets-the-shaving-gel-and-foam-market/ (accessed 3.17.19).

Deshpande, N.S., Barigou, M., 2001a. Flow of gas-liquid foams through pipe fittings. Int. J. Heat Fluid Flow 22, 94–101. https://doi.org/10.1016/S0142-727X(00)00075-8

Deshpande, N.S., Barigou, M., 2001b. Foam flow phenomena in sudden expansions and contractions. Int. J. Multiph. Flow 27, 1463–1477. https://doi.org/10.1016/S0301-9322(01)00017-9

Deshpande, N.S., Barigou, M., 2000. The flow of gas-liquid foams in vertical pipes. Chem. Eng. Sci. 55, 4297–4309. https://doi.org/10.1016/S0009-2509(00)00057-9

Dollet, B., 2010. Local description of the two-dimensional flow of foam through a contraction. J. Rheol. (N. Y. N. Y). 54, 741–760. https://doi.org/10.1122/1.3380852

Dollet, B., Elias, F., Quilliet, C., Raufaste, C., Aubouy, M., Graner, F., 2005. Two-dimensional flow of foam around an obstacle: Force measurements. Phys. Rev. E - Stat. Nonlinear, Soft Matter Phys. 71, 1–11. https://doi.org/10.1103/PhysRevE.71.031403

Dollet, B., Graner, F., 2007. Two-dimensional flow of foam around a circular obstacle: Local measurements of elasticity, plasticity and flow. J. Fluid Mech. 585, 181–211. https://doi.org/10.1017/S0022112007006830

Durian, D.J., 1997. Bubble-scale model of foam mechanics:mMelting, nonlinear behavior, and avalanches. Phys. Rev. E 55, 1739–1751. https://doi.org/10.1103/PhysRevE.55.1739

Eliceiri, K., Schneider, C.A., Rasband, W.S., Eliceiri, K.W., 2012. NIH Image to ImageJ : 25 years of image analysis. Nat. Methods 9, 671–675. https://doi.org/10.1038/nmeth.2089

Ferreira, T., Rasband, W., 2012. ImageJ User Guide User Guide IJ 1.46, 1–198.

Graner, F., Dollet, B., Raufaste, C., Marmottant, P., 2008. Discrete rearranging disordered patterns, part I: Robust statistical tools in two or three dimensions. Eur. Phys. J. E 25, 349–369. https://doi.org/10.1140/epje/i2007-10298-8

Jabarkhyl, S., Barigou, M., Badve, M., Zhu, S., 2020. Rheological properties of wet foams generated from viscous pseudoplastic fluids. Innov. Food Sci. Emerg. Technol. 102304. https://doi.org/10.1016/j.ifset.2020.102304

Jay, P., Magnin, A., Piau, J.M., 2002. Numerical Simulation of Viscoplastic Fluid Flows Through an Axisymmetric Contraction. J. Fluids Eng. 124, 700. https://doi.org/10.1115/1.1486472

Jones, S.A., Cox, S.J., 2012. On the effectiveness of a quasistatic bubble-scale simulation in predicting the constriction flow of a two-dimensional foam. J. Rheol. (N. Y. N. Y). 56,

457–471. https://doi.org/10.1122/1.3687301
Jones, S.A., Dollet, B., Slosse, N., Jiang, Y., Cox, S.J., Graner, F., 2011. Two-dimensional constriction flows of foams. Colloids Surfaces A Physicochem. Eng. Asp. 382, 18–23. https://doi.org/10.1016/j.colsurfa.2010.11.054
Langlois, V.J., 2014. The two-dimensional flow of a foam through a constriction: Insights from the bubble model. J. Rheol. (N. Y. N. Y). 58, 799–818. https://doi.org/10.1122/1.4872058
Lim, K.S., 2005. Studies of foam microstructure and rheology. PhD Thesis. University of Birmingham. United Kingdom.
Marmottant, P., Raufaste, C., Graner, F., 2008. Discrete rearranging disordered patterns, part II: 2D plasticity, elasticity and flow of a foam. Eur. Phys. J. E 25, 371–384. https://doi.org/10.1140/epje/i2007-10300-7
RAM, 2018. Global Polyurethane Foams Market Size, Market Share, Application Analysis, Regional Outlook, Growth Trends, Key Players, Competitive Strategies and Forecasts, 2018 To 2026 [WWW Document]. URL https://www.researchandmarkets.com/reports/4620334/global-polyurethane-foams-market-size-market (accessed 3.15.19).
RAM, 2013. Global Retail Ice Cream Industry 2013-2018: Trends, Profits and Forecast Analysis [WWW Document]. URL https://www.researchandmarkets.com/research/2n6zfd/global_retail_ice (accessed 3.15.19).
Thielicke, W., Stamhuis, E.J., 2014. PIVlab – Towards User-friendly, Affordable and Accurate Digital Particle Image Velocimetry in MATLAB. J. Open Res. Softw. 2. https://doi.org/10.5334/jors.bl
Wiggers, F.N., Deshpande, N.S., Barigou, M., 2000. The Flow of Foam Films in Vertical Tubes. Chem. Eng. Res. Des. 78, 773–778. https://doi.org/10.1205/026387600527789